JOURNAL OF GEOPHYSICAL RESEARCH, VOL. 100, NO. A4, PAGES 5599–5612, APRIL 1, 1995

# Modeling the Earth's magnetospheric magnetic field confined within a realistic magnetopause

N. A. Tsyganenko

Laboratory for Extraterrestrial Physics, Hughes STX Corporation, NASA Goddard Space Flight Center
Greenbelt, Maryland

**Abstract.** Empirical data-based models of the magnetospheric magnetic field have been widely used during recent years. However, the existing models (Tsyganenko, 1987, 1989a) have three serious deficiencies: (1) an unstable "de facto" magnetopause, (2) a crude parametrization by the $K_p$ index, and (3) inaccuracies in the equatorial magnetotail $B_z$ values. This paper describes a new approach to the problem; the essential new features are (1) a realistic shape and size of the magnetopause, based on fits to a large number of observed crossings (allowing a parametrization by the solar wind pressure), (2) fully controlled shielding of the magnetic field produced by all magnetospheric current systems, (3) new flexible representations for the tail and ring currents, and (4) a new "directional" criterion for fitting the model field to spacecraft data, providing improved accuracy for field line mapping. Results are presented from initial efforts to create models assembled from these modules and calibrated against spacecraft data sets.

## 1. Introduction

Quantitative data-based models of the distant geomagnetic field have become one of the essential tools for mapping the Earth's magnetosphere. They help to extract more information from large amounts of spacecraft measurements and make it possible to go beyond qualitative cartoons in describing the average configuration of geomagnetic field lines, which is crucial for the interpretation of ground and ionospheric phenomena [e.g., *Elphinstone et al.*, 1991] and for supporting spacecraft observations [*Baker et al.*, 1993]. Accurate magnetic field models are important for numerically tracing the orbits of solar energetic particles [*Bieber et al.*, 1992], for studying the dynamics of the magnetospheric plasma [e.g., *Spence et al.*, 1987; *Cao and Lee*, 1994], and in quantitative simulations of the substorm effects [e.g., *Pulkkinen et al.*, 1991].

The works listed above have employed the empirical data-based models of *Tsyganenko and Usmanov* [1982] and *Tsyganenko* [1987, 1989a]. Though widely used in recent years, these models have several deficiencies. First, they use an oversimplified method for representing the field from the magnetopause currents. In all of the above models, this field was approximated by sums of terms containing factors with exponential $X_{GSM}$ dependence, multiplied by polynomials in $Y_{GSM}$ and $Z_{GSM}$. The polynomial coefficients were fitted by least squares to large spacecraft data sets, and the model magnetopause appeared as a "de facto" surface that separated two families of field lines: those with at least one intersection with the Earth's surface and those with no connection to Earth. This approach is computationally feasible and yields a magnetopause with a fairly realistic shape and size in the front region $|X_{GSM}| \leq 10 - 15\, R_E$. However, farther down the tail the de facto magnetopause becomes unstable and deviates from its expected position, especially in the regions where data are sparse or absent. For large tilt angles of the Earth's dipole, there also emerge spurious "open" field lines near the polar cusps. All these features reflect a lack of explicit control over the shape the magnetopause and the distribution of the interconnection magnetic field on the boundary. No direct data on the magnetopause position were used in the models so far, and the de facto boundaries should be considered as a result of an outward extrapolation of the model field beyond the region covered by measurements.

The second limitation is related to the parametrizing of the model. In contrast to the internal field of the Earth, the extraterrestrial magnetospheric field is highly variable: in addition to small-scale irregularities and substorms, it exhibits large-scale changes due to varying solar wind pressure and effects of the interplanetary magnetic field. In the magnetic field models cited earlier, the only parameter used for quantifying the state of the magnetosphere was the $K_p$ index. This way of parametrizing a model, though crude, was convenient, since the $K_p$ index is available for any interval of time, while the solar wind data often are not. Note also that the $K_p$ index reflects (though in a very indirect manner) the actual degree of disturbance which already exists on Earth and in the surrounding space; by contrast, the current solar wind state (especially the IMF) appears, to some extent, as a potential factor, since it induces both immediate (directly driven) and delayed (loading-unloading) effects. However, in view of the 3-hour resolution of the $K_p$ index and the fact that it mixes together effects of several physical processes, it is clear that the models need a better method for quantifying the magnetospheric conditions.



Paper number 94JA03193.
0148-0227/95/94JA-03193$05.00

The third problem, encountered in studies of the nightside magnetic field configurations, is a poor fit to observations by predicted model values of the equatoral $B_z$ in the tail plasma sheet. According to our earlier result [*Tsyganenko*, 1989a], as well as that of an independent study of *Fairfield* [1991], the models based on a quasi-two-dimensional representation of the field from the tail current sheet [*Tsyganenko and Usmanov*, 1982; *Tsyganenko*, 1987] significantly underestimate the field line stretching in the inner magnetosphere. On the other hand, at larger tailward distances the more recent model [*Tsyganenko*, 1989a] yielded values of equatorial $B_z$ that were too small, or even negative, especially for quiet conditions. This drawback was mentioned in the original paper and was discussed in detail in several later works [*Stern and Tsyganenko*, 1992; *Donovan et al.*, 1992; *Rostoker and Skone*, 1993; *Peredo et al.*, 1993; *Huang and Frank*, 1994]. There are two basic reasons for the problems with the equatorial tail $B_z$. The first stems from the fact that the net $B_z$ in the near plasma sheet ($-30 \leq X \leq -5R_E$) is a relatively small sum of two terms having large absolute values and opposite signs. The first term is the northward field $B_z^{\mathrm{dip}} + B_z^{\mathrm{DS}}$, produced by the Earth's dipole and the dipole-shielding (Chapman-Ferraro) currents, while the second term, $B_z^T$, is the southward contribution from the tail current sheet. Therefore the net $B_z$ is very sensitive to variations in both the magnetopause and tail current, so that even relatively small changes in the tail current intensity and/or geometry can produce large effects with regard to $B_z$. The second source of the $B_z$ problem lies in the mathematical procedure for deriving the model parameters and also in the uneven coverage of the modeling region by spacecraft data. As is discussed in more detail in section 3, the standard least squares criterion employed in previous studies tends to optimize the model for the tail lobes at the expense of the fit in the plasma sheet, which significantly reduces the mapping accuracy there.

The purpose of this paper is to present initial results of recent efforts to develop a new data-based model, free from the drawbacks discussed above. Section 2 will describe methods for modeling the field of magnetopause currents; that field is resolved into several components, each of which arises in response to one of the current systems in the interior. Section 3 will present first results of assembling the fully shielded modules of the model, using new mapping-oriented optimization criteria. Section 4 will discuss prospects for parametrizing the model by solar wind parameters and is followed by a brief summary.

## 2. Derivation of the Magnetopause Field for Realistic Model Boundaries

Since the pioneering works of *Midgeley and Davis* [1963] and *Mead and Beard* [1964], the problem of representation of the magnetopause magnetic field has been addressed by many authors (see the review by *Tsyganenko* [1990] for a comprehensive list of references). Nowadays, the preferred approach is to specify an appropriate analytical boundary and represent the magnetopause field inside the magnetosphere by using a scalar potential. Given a distribution of the net normal component $B_n$ at the magnetopause (zero in the case of a fully closed model), the potential can be derived by solving a Neumann problem. This method was used in several studies; however, until recently, it was applied mainly to the case of shielding the Earth's dipole field [*Alekseev and Shabansky*, 1972; *Voigt*, 1972; *Tsyganenko*, 1989b]. *Stern* [1985] obtained the shielding potential for a simple model of the ring current as well. In a general case, the field of any internal magnetospheric source, including the cross-tail current sheet and the large-scale Birkeland current system, induces its own shielding currents at the magnetopause, which should also be taken into account. A special problem with the cross-tail current (and, probably, with the region 1 Birkeland current) is that its path does not lie entirely inside the magnetosphere; instead, it extends up to the boundary and forms there a closure circuit, contributing thus to the shielding current [*Sotirelis et al.*, 1994].

*Voigt* [1981] circumvented this difficulty by constructing a shielded taillike field as a product of a tailward stretch imposed on a shielded dipole field. This method provided visually reasonable configurations, in which the degree of the field line deformation could be easily varied to simulate changes of the magnetotail geometry. However, stretch transformations give rise to spurious electric currents, and there is no simple way to keep them under control. As a result, models of that kind cannot correctly reproduce global effects of the tail current [*Tsyganenko*, 1990].

In the works cited above, the magnetopause shape was approximated by simple analytical surfaces (paraboloid, cylinder capped with a hemisphere, and ellipsoid). That imposed limitations on the shape of the model surface but, because of the existence of specific harmonic functions associated with the given shape, allowed an easy derivation of the coefficients of the corresponding expansions, using the orthogonality of eigenfunctions. *Toffoletto et al.* [1994] suggested a numerical solution for confining the dipole and cross-tail current fields within an arbitrary boundary. However, that method pays a high price by requiring a large array of numerical values on a two-dimensional grid and an interpolation between them, to determine the field components at an arbitrary point in space.

Fortunately, there exists an alternative approach that combines both features we need: arbitrary shape of the boundary and the possibility of compactly representing the scalar potential as an expansion in a suitable set of harmonic functions. This method was proposed by *Schulz and McNab* [1987] but has not been duly appreciated so far. Its essence consists in replacing the strict boundary condition imposed on the normal component of the magnetic field by a weaker one, requiring the condition to be satisfied only in a mean square sense.

In this work the method of Schulz and McNab is used for constructing shielding potentials for the Earth's dipole, the ring current, and the cross-tail current sheet. Each source requires a separate choice of appropriate expansion functions, based on specific properties of the original field. In all cases we were able to construct very accurate solutions, even with relatively small numbers of expansion terms.

### 2.1. The Shape of the Model Magnetopause

The approximate "source-surface" method gives us a great freedom in choosing appropriate model boundaries and there-

fore allows to use shapes derived by statistical studies of direct observations of magnetopause crossings. The first such study was done by *Fairfield* [1971], who derived a best fit ellipsoid surface from several hundred magnetopause positions observed by IMP spacecraft. Two decades later, *Sibeck et al.* [1991], *Petrinec et al.* [1991], and *Roelof and Sibeck* [1993] performed more detailed studies in which the effects of the solar wind pressure and of the IMF $B_z$ were addressed. *Petrinec and Russell* [1993] introduced an indirect technique of remotely inferring the tail magnetopause shape from lobe field data, using an approximate pressure balance equation. These works provided a good quantitative basis for modeling the magnetopause down to 30–40 $R_E$ tailward. There is much less experimental information on the magnetopause radius and flaring rate at larger distances. *Behannon* [1970] and *Maezawa* [1975] estimated the average tail radius near the Moon's orbit as 25–30 $R_E$; the same estimate was obtained by *Howe and Binsack* [1972], who fitted an axially symmetric surface to then available spacecraft data.

On the basis of these above results, we assumed a composite shape for the average magnetopause, a prolate hemiellipsoid of revolution in the front (up to tailward distance of 60–70 $R_E$), smoothly continued in the far tail by a cylindrical surface, as shown in Figure 1. Following the notation of *Tsyganenko* [1989b], the ellipsoidal part of the boundary is given by

$$\begin{aligned} X &= x_0 - a(1-\sigma_0\tau) \\ Y &= a(\sigma_0^2-1)^{1/2}(1-\tau^2)^{1/2}\cos\phi \\ Z &= a(\sigma_0^2-1)^{1/2}(1-\tau^2)^{1/2}\sin\phi \end{aligned} \qquad (1)$$

where $X$, $Y$, and $Z$ are the GSM coordinates and the ellipsoidal coordinates $\tau$ and $\phi$ span the intervals $0 \le \tau \le 1$ and $0 \le \phi \le 2\pi$, respectively. The parameters $x_0$, $a$, and $\sigma_0$ can be derived from the results of *Sibeck et al.* [1991] and *Roelof and Sibeck* [1993], who also modeled the magnetopause by axially symmetric ellipsoids but used a different mathematical form, namely, $g(\mathbf{r}) = AX^2 + BX + C + Y^2 + Z^2 = 0$. The relationship between the parameters $A$, $B$, and $C$ and those in (1), is as follows:

$$\begin{aligned} \sigma_0 &= (1-A)^{-1/2} \\ a &= \left\{\left[\left(\frac{B}{2A}\right)^2 - \frac{C}{A}\right](1-A)\right\}^{1/2} \\ x_0 &= a - \frac{B}{2A} \end{aligned} \qquad (2)$$

In this study we used the values $x_0 = 5.48\,R_E$, $a = 70.48\,R_E$, and $\sigma_0 = 1.078$, which correspond to $A = 0.14$, $B = 18.2$, and $C = -217.2$, given by *Sibeck et al.* [1991] for the intermediate range of the solar wind pressure values $1.47 \le p_{\rm dyn} \le 2.60$ nPa.

Another useful set of formulas relates the standoff distance $R_S$, the terminator magnetopause radius $R_D$, and the asymptotic tail radius $R_T$ with the aforementioned parameters $x_0$, $a$, and $\sigma_0$:

$$\begin{aligned} R_S &= x_0 + a(\sigma_0 - 1) \\ R_D &= \sqrt{R_S(1-\sigma_0^{-2})(2a\sigma_0 - R_S)} \\ R_T &= a\sqrt{\sigma_0^2 - 1} \end{aligned} \qquad (3)$$

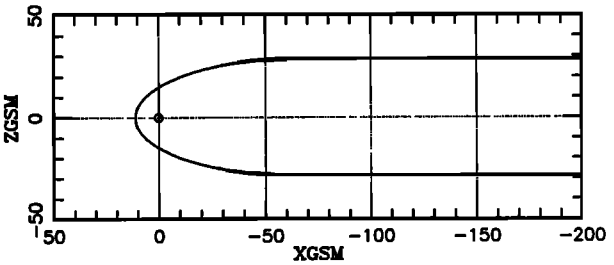


**Figure 1.** Noon-midnight meridian section of the model magnetopause. The axially symmetric boundary is composed of a hemiellipsoid, smoothly continued by a cylinder beyond the Moon's orbit. The size and shape of the magnetopause correspond to intermediate range of the solar wind dynamic pressure, $1.47 \le p_{\rm sw} \le 2.60$ nPa, as given by *Sibeck et al.* [1991].

The corresponding numerical values for these quantities are $R_S = 10.98\,R_E$, $R_D = 14.69\,R_E$, and $R_T = 28.38\,R_E$.

### 2.2. The Scalar Potential

We now seek a potential magnetic field $\mathbf{B}^{\rm MP} = -\nabla U$ produced by magnetopause currents, which, when added to the field $\mathbf{B}^{\rm int}$ from an internal source, provides the required distribution of the net normal component $B_n$ at the model boundary $S$. The potential $U$ can be derived by solving the Neumann's problem

$$\begin{aligned} &\nabla^2 U = 0 \\ &\left.\frac{\partial U}{\partial n}\right|_S - B_n^{\rm int} + B_n = 0 \end{aligned} \qquad (4)$$

The first step is to choose an appropriate analytical representation for the scalar potential $U$. In contrast with the approach based on exact solutions [e.g., *Stern*, 1985; *Tsyganenko*, 1989b], no restrictions are imposed on the choice of eigenfunctions: any harmonic potential with a sufficient number of free parameters can be used. A practical way of constructing flexible scalar potentials is to use the expansions

$$U = \sum_{i,k} a_i\,\chi(b_k, \mathbf{r})$$

containing variable amplitude coefficients $a_i$ as well as nonlinear parameters $b_k$, which may enter into the separate harmonics $\chi(b_k, \mathbf{r})$ as scale, shift, and/or rotation factors.

Following *Schulz and McNab* [1987], we replace the boundary condition in (4) by a requirement of a minimum mean square of the residual normal field in the vector space $\{\mathbf{a}, \mathbf{b}\}$ of the parameters $a_i$ and $b_i$:

$$\min_{\{\mathbf{a},\mathbf{b}\}} \int_S \left\{\frac{\partial U(\mathbf{a},\mathbf{b},\mathbf{r}_s)}{\partial n} - B_n^{\rm int}(\mathbf{r}_s) + B_n(\mathbf{r}_s)\right\}^2 ds \qquad (5)$$

In practice, the integration in (5) can be replaced by summation over a set of $K$ points having a sufficiently even distribution on the model magnetopause, so that the quantity to be minimized is

$$\langle \delta B_n^2 \rangle = \frac{1}{K}\sum_{k=1}^{K}\left\{\frac{\partial U}{\partial n} - B_n^{\rm int}(\mathbf{r}_k) + B_n(\mathbf{r}_k)\right\}^2 \qquad (6)$$

As is described below, this approach has been successfully implemented to derive analytical potentials for the case of full shielding ($B_n = 0$) of principal sources of the magnetospheric magnetic field.

### 2.3. Shielding of the Earth's Dipole Field

Shielding of the dipole source is the simplest case, due to the following special properties of the dipole field [e.g., *Tsyganenko*, 1990]. First, the magnetic moment **M** of a dipole tilted by the angle $\Psi$ with respect to the $Z$ axis can be represented as

$$\mathbf{M} = \mathbf{M}^{\parallel} + \mathbf{M}^{\perp} = M\,(\hat{\mathbf{e}}_x \sin\Psi + \hat{\mathbf{e}}_z \cos\Psi) \qquad (7)$$

and therefore the potential for an arbitrary $\Psi$ can be reduced to a linear combination of solutions for $\Psi = 90°$ and $\Psi = 0°$.

Second, in the case of axially symmetric boundaries, the normal component $B_n^{\rm dip}$ on the surface either varies as $\sin\phi$, where $\phi = \tan^{-1}(Z/Y)$, or does not depend on $\phi$ at all, for the cases $\Psi = 0°$ and $\Psi = 90°$, respectively. With a proper choice of fitting potentials, this permits us to reduce the dimensionality of the problem from 2 to 1; in other words, it suffices to minimize $\langle \delta B_n^2 \rangle$ on a line rather than on a surface.

What harmonic functions are the most appropriate for shielding the dipole? Spherical harmonics, used by *Mead* [1964], *Choe and Beard* [1974], and *Schulz and McNab* [1987], rapidly diverge with increasing geocentric distance and provide satisfactory results only for $R < 8$–$10\,R_E$. Ellipsoidal harmonics [*Tsyganenko*, 1989b] have appropriate behavior up to 40–60 $R_E$ tailward; however, they are equivalent to combinations of high-order polynomials of Cartesian coordinates and hence become unstable at larger distances. Other candidates are the parabolic [*Alekseev and Shabansky*, 1972; *Stern*, 1985] and cylindrical [*Voigt*, 1972; *Beard et al.*, 1982] harmonics. The parabolic harmonics decay in the antisunward direction; however, there arise numerical problems at the dayside, close to the focus of the paraboloid. For that reason, in this work preference was given to the cylindrical harmonics, which have the desired behavior at both small and large distances and are the most feasible ones from the computational viewpoint.

At an early phase of this work, the expansions

$$U^{\perp} = \sum_{i=1}^{N} A_i\, J_1(\tfrac{\rho}{b_i})\, \exp(\tfrac{X}{b_i})\, \sin\phi \qquad (8)$$

$$U^{\parallel} = \sum_{i=1}^{N} C_i\, J_0(\tfrac{\rho}{d_i})\, \exp(\tfrac{X}{d_i}) \qquad (9)$$

with $N$=5–7 terms were explored for the cases $\Psi = 0°$ and $\Psi = 90°$, respectively. Optimal values for the nonlinear parameters $b_i$ and $d_i$ were searched out by using the downhill simplex algorithm [*Press et al.*, 1992], while the coefficients $A_i$ and $C_i$ were determined at each step by a standard matrix inversion procedure. The "merit function" (6) was minimized on a set of $K$=175 points, distributed between the subsolar point and $X \approx -350\,R_E$ on the line of intersection of the model magnetopause and the noon-midnight meridian plane (taking advantage of the matching in the $\phi$ dependence between the dipole field and cylindrical harmonics). A denser distribution of points was used in the front region, which lie closer to the dipole and therefore have larger $B_n^{\rm dip}$ than those at large tailward distance. Even for such a relatively small number of terms, a very good quality of shielding was obtained, with typical values of $\langle \delta B_n^2 \rangle^{1/2}$ as low as 0.001 nT and maximal $|B_n|$ not exceeding 0.003–0.005 nT. Later it was found that some of the nonlinear parameters $b_i$ and $d_i$ tended to cluster in close pairs in the course of iterations, while the corresponding coefficients $A_i$ and $C_i$ took opposite signs and rapidly grew in magnitude. That suggested a need to include in the expansions (8) and (9) "derivative" terms, obtained from the original cylidrical harmonics by differentiating with respect to the parameters $b_i$ and $d_i$, which yields $U^{\perp\prime} \sim [\rho\, J_0(\rho/b_i) + (X - b_i)\, J_1(\rho/b_i)]\, \exp(X/b_i)\, \sin\phi$ and $U^{\parallel\prime} \sim [X\, J_0(\rho/d_i) - \rho\, J_1(\rho/d_i)]\, \exp(X/d_i)$. By construction, these additional terms are also harmonic functions, but in contrast to the original cylindrical harmonics, they have a nonmonotonic variation with $X$ and therefore increase the flexibility of the model potential.

Finally, six-term expansions were adopted for the potentials $U^{\perp}$ and $U^{\parallel}$, each containing three "original" and three "derivative" cylindrical harmonics. After some algebra and denoting $a_i = A_i/b_i$, $c_i = C_i/d_i$, the corresponding final expressions for the magnetic field components in the cylindrical coordinates $\rho = (Y^2 + Z^2)^{1/2}$, $\phi = \tan^{-1}(Z/Y)$, and $X$, read as follows:

$$B_x^{\perp} = \sin\phi \Big\{ -\sum_{i=1}^{3} a_i\, \exp(\tfrac{X}{b_i})\, J_1(\tfrac{\rho}{b_i}) + \sum_{i=4}^{6} \tfrac{a_i}{b_i}\, \exp(\tfrac{X}{b_i}) \left[ \rho\, J_0(\tfrac{\rho}{b_i}) + X\, J_1(\tfrac{\rho}{b_i}) \right] \Big\} \qquad (10)$$

$$B_{\rho}^{\perp} = \sin\phi \Big\{ \sum_{i=1}^{3} a_i\, \exp(\tfrac{X}{b_i}) \left[ J_1(\tfrac{\rho}{b_i})/(\tfrac{\rho}{b_i}) - J_0(\tfrac{\rho}{b_i}) \right] + \sum_{i=4}^{6} a_i\, \exp(\tfrac{X}{b_i}) \left[ \tfrac{X}{b_i}\, J_0(\tfrac{\rho}{b_i}) - (\tfrac{\rho^2}{b_i^2} + \tfrac{X}{b_i} - 1)\, J_1(\tfrac{\rho}{b_i})/(\tfrac{\rho}{b_i}) \right] \Big\} \qquad (11)$$

$$B_{\phi}^{\perp} = \cos\phi \Big\{ -\sum_{i=1}^{3} a_i\, \exp(\tfrac{X}{b_i})\, J_1(\tfrac{\rho}{b_i})/(\tfrac{\rho}{b_i}) + \sum_{i=4}^{6} a_i\, \exp(\tfrac{X}{b_i}) \left[ J_0(\tfrac{\rho}{b_i}) + \tfrac{X - b_i}{b_i}\, J_1(\tfrac{\rho}{b_i})/(\tfrac{\rho}{b_i}) \right] \Big\} \qquad (12)$$

$$B_x^{\parallel} = -\sum_{i=1}^{3} c_i\, \exp(\tfrac{X}{d_i})\, J_0(\tfrac{\rho}{d_i}) + \sum_{i=4}^{6} c_i\, \exp(\tfrac{X}{d_i}) \left[ \tfrac{\rho}{d_i}\, J_1(\tfrac{\rho}{d_i}) - \tfrac{X + d_i}{d_i}\, J_0(\tfrac{\rho}{d_i}) \right] \qquad (13)$$

$$B_\rho^{\parallel} = -\sum_{i=1}^{3} c_i \exp(\frac{X}{d_i})\, J_1(\frac{\rho}{d_i}) + \sum_{i=4}^{6} \frac{c_i}{d_i} \exp(\frac{X}{d_i}) \left[\rho\, J_0(\frac{\rho}{d_i}) + X\, J_1(\frac{\rho}{d_i})\right] \quad (14)$$

$$B_\phi^{\parallel} = 0 \quad (15)$$

For a given value of the Earth's dipole tilt angle $\Psi$, the components of the dipole-shielding field can be found by using (10–15) as

$$\mathbf{B}_{DS} = \mathbf{B}^{\perp} \cos\Psi + \mathbf{B}^{\parallel} \sin\Psi \quad (16)$$

The 24 parameters $a_i$,$b_i$,$c_i$, and $d_i$ ($i = 1, 2, \ldots, 6$) were computed for the average model magnetopause shown in Figure 1. For completeness, several sets of parameters were found, corresponding to boundaries with different rates of tailward flaring. More specifically, the boundaries were obtained from the "base" model magnetopause with $x_0 = 5.48\,R_E$, $a = 70.48\,R_E$, and $\sigma_0 = 1.078$, shown in Figure 1, by a transverse scaling of $R_T$ and $R_D$ in (3) by a factor $1 + \epsilon$, keeping $R_S = 10.98\,R_E$ as before, but making appropriate changes in $x_0$, $a$, and $\sigma_0$. Table 1 gives the values of the shielding field parameters for 7 values of $\epsilon$, including the case $\epsilon = 0$ of the base model. Figure 2 displays three configurations of the magnetic field lines, corresponding to $\epsilon = 0$ (Figure 2a), base model with $R_T = 28.38 R_E$; $\epsilon = -0.15$ (Figure 2b), providing a "sharper" magnetopause with a smaller tail radius $R_T = 24.12\,R_E$; and $\epsilon = 0.15$ (Figure 2c), for a blunter boundary with $R_T = 32.64\,R_E$. In all cases the standoff distance and the position of the "seam" between the ellipsoidal and cylindrical parts of the boundary remained the same, equal to $R_S = 10.98\,R_E$ and $X_M = -65\,R_E$, respectively.

The easiest way to extend the results given above to different standoff distances is to apply a uniform scaling transformation to the field (16), that is, use

$$\mathbf{B}'_{DS}(\mathbf{r}) = \kappa^3\, \mathbf{B}_{DS}(\kappa \mathbf{r}) \quad (17)$$

for the shielding field inside a magnetopause, uniformly compressed/expanded by a factor $\kappa$. The modified field $\mathbf{B}'_{DS}(\mathbf{r})$ is also curl-free and satisfies the shielding condition on the new boundary. Superposing the two transformations allows one to model the dipole shielding field for a wide variety of possible average boundary shapes.

### 2.4. Shielding of the Magnetotail Field

It is much harder to find a solution to the shielding problem for the case of the cross-tail current than for the geodipole. First, the tail field no longer varies as $\sin\phi$ along the circles in the $Y$-$Z$ plane, as the dipole field does. Instead, the $B_x$ component abruptly reverses its direction as the observation point crosses the equatorial current sheet. This means that the shielding scalar potential should contain higher-order harmonics of the angle $\phi$, which requires many more parameters in the fitting algorithm. Adding to that complication, the least squares fitting can no longer be reduced to a one-dimensional minimization, and hence the sum (6) must include points scattered over the entire surface, rather than on a single line.

**Table 1.** Values of the Parameters of the Dipole-Shielding Field (Equations (10)–(16)), for Seven Values of the Flaring Parameter $\epsilon$

| $\epsilon$ | −0.15 | −0.10 | −0.05 | 0.0 | 0.05 | 0.10 | 0.15 |
|---|---|---|---|---|---|---|---|
| $a_1$ | 2.3201 | 0.56459 | 0.34613 | 0.24777 | 0.18550 | 0.15401 | 0.36944 |
| $a_2$ | −33.817 | −32.997 | −30.219 | −27.003 | −24.064 | −21.183 | −12.109 |
| $a_3$ | −7.3791 | −2.6020 | −1.0478 | −0.46815 | −0.27494 | −0.87867 | −9.8385 |
| $a_4$ | 16.116 | 10.385 | 8.1492 | 7.0637 | 6.3689 | 5.8432 | 3.4316 |
| $a_5$ | −7.1853 | −4.1069 | −2.5606 | −1.5918 | −0.95028 | −0.82001 | −0.29360 |
| $a_6$ | −1.5378 | −0.53885 | −0.21156 | −0.090317 | −0.04663 | −0.00001 | 0.0094316 |
| $b_1$ | 29.804 | 43.053 | 50.903 | 57.522 | 64.173 | 68.687 | 51.044 |
| $b_2$ | 15.255 | 13.352 | 13.333 | 13.757 | 14.304 | 15.039 | 19.087 |
| $b_3$ | 2.0426 | 2.0078 | 1.9951 | 2.0100 | 2.1399 | 3.3004 | 8.0832 |
| $b_4$ | 11.171 | 10.476 | 10.347 | 10.458 | 10.648 | 11.003 | 14.413 |
| $b_5$ | 4.0723 | 4.3181 | 4.4983 | 4.5798 | 4.5269 | 4.3373 | 4.5040 |
| $b_6$ | 2.2204 | 2.1807 | 2.1619 | 2.1695 | 2.2849 | 1.5656 | 3.0303 |
| $c_1$ | −24.634 | −0.34300 | −0.53887 | −0.65385 | −0.70835 | −0.74268 | −0.26542 |
| $c_2$ | 49.046 | −21.271 | −19.771 | −18.061 | −16.408 | −14.938 | −11.590 |
| $c_3$ | −63.008 | −2.5562 | −0.98885 | −0.40457 | −0.17071 | −0.085853 | 0.73751 |
| $c_4$ | −13.179 | −8.4702 | −6.4572 | −5.0995 | −4.1943 | −3.5410 | −4.0315 |
| $c_5$ | 8.7750 | 3.3336 | 2.0427 | 1.2846 | 0.78142 | 0.44164 | −2.1084 |
| $c_6$ | 10.160 | 0.52528 | 0.19881 | 0.078231 | 0.030995 | 0.01240 | −0.075475 |
| $d_1$ | 14.853 | 51.081 | 42.571 | 39.592 | 38.437 | 37.768 | 53.490 |
| $d_2$ | 3.1900 | 14.089 | 13.516 | 13.291 | 13.260 | 13.281 | 17.212 |
| $d_3$ | 2.2795 | 2.0196 | 2.0013 | 1.9970 | 2.0136 | 2.1681 | 3.3504 |
| $d_4$ | 10.307 | 10.419 | 10.177 | 10.062 | 10.012 | 9.9545 | 13.382 |
| $d_5$ | 3.1708 | 4.1867 | 4.3853 | 4.5140 | 4.5538 | 4.4771 | 8.7610 |
| $d_6$ | 2.4347 | 2.1922 | 2.1678 | 2.1558 | 2.1626 | 2.2865 | 3.3459 |

The case $\epsilon = 0$ corresponds to the average magnetopause shape and size for $1.47 \leq p_{sw} \leq 2.60$ nPa, as given by *Sibeck et al.* [1991].

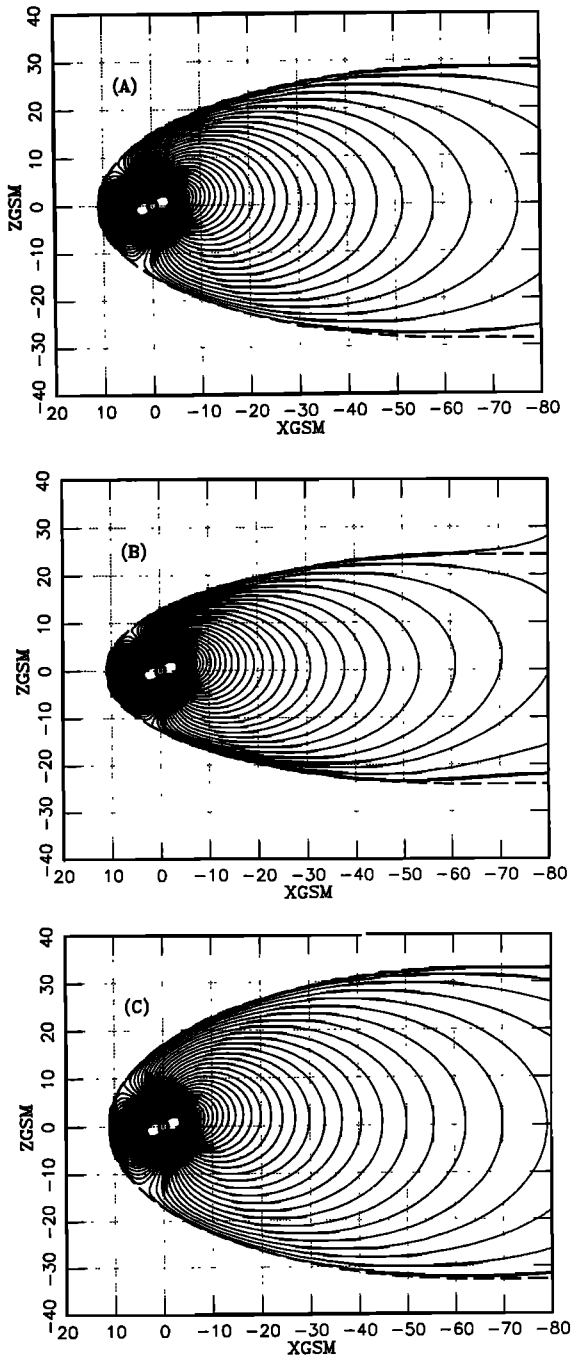


**Figure 2.** Magnetic field lines of the Earth's dipole field, confined within the model magnetopause by addition of the shielding field (equations (10)–(16)). The three panels display the field configurations with the same standoff distance, but having different rates of the tailward flaring of the model magnetopause (dashed line), quantified by the transverse scaling parameter $\epsilon$: (a) $\epsilon = 0$, corresponding to the unchanged magnetopause shape of Figure 1, (b) $\epsilon = -0.15$, yielding a sharper boundary shape, and (c) $\epsilon = 0.15$, giving a blunter magnetopause. In all the three cases, the dipole tilt angle $\Psi = 25°$.

Second, the effect of the geodipole tilt, which by (7) and (16) reduces to a simple superposition for the dipole shielding field, is much more complicated for the tail. We actually do not know exactly how the tail current sheet behaves in response to the Earth's dipole tilt, but we use various approximations for describing its two-dimensional warping, which parameters are determined from data. The latter fact also implies that the tail-shielding field must be iteratively adjusted in the course of a search of the cross-tail field parameters.

Before we proceed to the tail-shielding problem, a brief description of the model used for the cross-tail equatorial current sheet is given below. Readers are referred to the original paper [*Tsyganenko and Peredo*, 1994] for more details.

**2.4.1. The cross-tail current model.** In this work, a new model of the field of the cross-tail current [*Tsyganenko and Peredo*, 1994] is employed. Unlike earlier models [*Tsyganenko and Usmanov*, 1982; *Tsyganenko*, 1987, 1989a], it provides better representation of the observed features, including a gradual merging of the cross-tail and ring currents as well as a steep variation of the current density at the inner edge of the current sheet. The model allows the superposition of several independent "modes" with different rates of tailward decrease of the current density, and these can be mixed in variable proportions to achieve a best fit to data.

The model field is specified by means of a vector potential $\mathbf{A} = A_\phi \hat{\mathbf{e}}_\phi$, from which the magnetic field components can be derived in a straightforward way. We use a cylindrical coordinate system $\{\rho, \phi, Z\}$, whose origin is shifted by $X_c$ along the Sun-Earth direction, so that

$$\begin{aligned} \rho &= [(X - X_c)^2 + Y^2]^{1/2} \\ \phi &= \tan^{-1}[Y/(X - X_c)] \end{aligned} \tag{18}$$

In these coordinates the azimuthal component of the vector potential reads

$$A_\phi = \rho \sum_{i=1}^{N} f_i \frac{t_i \sqrt{1 - t_i^2}}{S_i^{(1)} S_i^{(2)}} \tag{19}$$

where

$$t_i = \frac{2b_i}{S_i^{(1)} + S_i^{(2)}} \tag{20}$$

$$S_i^{(1)} = \sqrt{[b_i + \zeta(Z, Z_s, D)]^2 + (\rho + g_i)^2} \tag{21}$$

$$S_i^{(2)} = \sqrt{[b_i + \zeta(Z, Z_s, D)]^2 + (\rho - g_i)^2} \tag{22}$$

The function $\zeta(Z, Z_s, D)$, entering in (21)–(22), is a smooth substitute for $Z_r = |Z - Z_s|$, providing a controlled finite thickness of the current sheet [*Tsyganenko and Peredo*, 1994]:

$$\begin{aligned} \zeta &= Z_r & Z_r > D \\ \zeta &= 0.5\,(Z_r^2/D + D) & Z_r \le D \end{aligned} \tag{23}$$

where $Z_s = Z_s(X, Y, \Psi)$ and $D = D(X, Y)$ describe the tilt-dependent shape of the current sheet and the variation of its thickness along and across the tail.

Before we specify the functions $Z_s$ and $D$, note that the vector potential (19) is a superposition of $N$ terms ($N = 7$ in the final version), each of which produces a magnetic field of some disclike axisymmetric equatorial current sheet. The weight coefficients $f_i$ and nonlinear parameters $g_i$ ensure a proper radial distribution of the current density, with a spread-out inner edge and a gradual outward decay. A nat-

ural question arises then: why can this axisymmetric current disc approximate the observed cross-tail current, which flows from dawn to dusk and then closes via the boundary closure current? The answer is as follows [*Sotirelis et al.*, 1994; *Stern*, 1994, section 5]. Suppose we have derived a curl-free shielding field which, when added to the field of the current disc, provides $B_n = 0$ everywhere on the model boundary. After that, we can remove the external field outside the magnetopause, i.e., set $\mathbf{B} \equiv 0$ there, without having violated any of Maxwell's equations (which, in particular, imply continuity of $B_n$ across the boundary). As a result, the external part of the current disc disappears. At the same time, having eliminated the exterior magnetic field, we introduce a jump in the tangential component of $\mathbf{B}$ and hence a surface current which, by $\nabla \cdot \mathbf{j} = 0$ (implied by Maxwell's equations), automatically serves as a closure current for the remaining intramagnetospheric segment of the cross-tail current.

Following the approach adopted in earlier models, the shape of the current sheet was specified through the function $Z_s(X, Y, \Psi)$, composed of two terms,

$$Z_s(X, Y, \Psi) = Z_s^{(1)}(X, \Psi) + Z_s^{(2)}(Y, \Psi) \tag{24}$$

simulating separately the current sheet deformations in the $X$–$Z$ and $Y$–$Z$ planes. The first term

$$Z_s^{(1)}(X, \Psi) = 0.5 \tan\Psi \left[\sqrt{(X - R_H \cos\Psi)^2 + (\Delta X \cos\Psi)^2} - \sqrt{(X + R_H \cos\Psi)^2 + (\Delta X \cos\Psi)^2}\right] \tag{25}$$

contains two parameters: the "hinging distance" $R_H$ and the scale distance $\Delta X$ defining the width of the transition region between the near-Earth and tailward parts of the current sheet. The second term

$$Z_s^{(2)}(Y, \Psi) = -G \sin\Psi \frac{Y^4}{Y^4 + L_w^4} \tag{26}$$

has the same form as in the earlier model [*Tsyganenko*, 1989a], where the coefficient $G$ controls the amplitude of the current sheet warping in the $Y$–$Z$ plane and the scale length $L_w$ defines its extension in the dawn-dusk direction.

Spatial variation of the sheet half thickness, $D(X, Y)$, was modeled in a similar way, as a sum of three terms

$$D(X, Y) = D_0 + D_x f_x(X) + D_y f_y(Y) . \tag{27}$$

The coefficients $D_0$, $D_x$, and $D_y$ define the sheet's half thickness in the midnight meridian plane and amplitudes of its variation in the $X$ and $Y$ directions, respectively, while the functions $f_x$ and $f_y$ were chosen as

$$\begin{aligned} f_x &= 0 && X < X_D \\ f_x &= \frac{(X - X_D)^2}{(X - X_D)^2 + L_x^2} && X > X_D \end{aligned} \tag{28}$$

and

$$f_y = \frac{Y^2}{Y^2 + L_y^2} \tag{29}$$

Of course, many alternative analytical forms can be chosen for specifying the configuration of the current sheet. The present choice, (24)–(29), is based on our previous experience in modeling the tail current. For example, one persistent feature of the 1989 model was a rapid thickening of the current sheet toward its dawn and dusk flanks, and taking out that degree of freedom led to a poorer agreement with data.

The preceding representation fully defines the current sheet geometry and contains, in total, 10 nonlinear parameters: 4 in the function $Z_s(X, Y, \Psi)$ and 6 in $D(X, Y)$. In this study, we used a combination of three vector potentials (19) for representing the field of the tail current sheet, with different scales of the tailward decrease of the electric current [*Tsyganenko and Peredo*, 1994]. The net cross-tail field is then a sum

$$\mathbf{B}_{CT} = a_{T,1}\,\mathbf{B}_{CT,1} + a_{T,2}\,\mathbf{B}_{CT,2} + a_{T,3}\,\mathbf{B}_{CT,3} \tag{30}$$

contributed by vector potentials of the form (19), with the scale lengths $L = 100\,R_E$, $40\,R_E$, and $15\,R_E$, respectively, and with variable amplitude factors $a_{T,1}$, $a_{T,2}$, and $a_{T,3}$. All three modes share the same 10 geometrical parameters, appearing in $Z_s$ and $D$. Additional degrees of freedom can be gained by introducing a variable shift $X_c$ of the tail and ring currents, as defined by (18), and allowing for a uniform scaling of the magnetic fields by a variable factor. We will further discuss this point in section 4.

**2.4.2. Scalar potentials for shielding the tail field.** As was already mentioned, the tail shielding potential should contain higher-order ($m > 1$) terms with $\sin m\phi$ and $\cos m\phi$, to properly match the field reversal between the lobes. An obvious solution is to use general series of cylindrical harmonics, that is, to expand (8)–(9) to include the terms

$$\begin{matrix} J_m(\rho/b_i)\,\exp(X/b_i)\,\sin m\phi \\ J_m(\rho/b_i)\,\exp(X/b_i)\,\cos m\phi \end{matrix} \tag{31}$$

with $m > 1$. This approach was pursued at an earlier stage of this work, and it was found that the cylindrical harmonics with $m \leq 7$ provided a fairly good shielding and, at the same time, a manageable number of expansion terms. However, although we retained the cylindrical harmonics for shielding the ring current (section 2.5), a simpler class of functions was later used for the tail shielding field, namely, the rectangular harmonics produced by separating Laplace's equation (4) in Cartesian coordinates:

$$U \propto \exp(X\sqrt{\alpha^2 + \beta^2}) \begin{Bmatrix} \cos\alpha Y \\ \sin\alpha Y \end{Bmatrix} \cdot \begin{Bmatrix} \cos\beta Z \\ \sin\beta Z \end{Bmatrix} \tag{32}$$

Like cylindrical harmonics, the rectangular harmonics decay exponentially tailward, but they contain just sines and cosines of the scaled coordinates $Y$ and $Z$, rather than Bessel functions.

A linear combination of the harmonics (32), sharing a single array of scale lengths $p_i$, was chosen as a basic potential for shielding the field of the cross-tail current sheet:

$$U = \sum_{i,k}^{N} a_{ik} \exp\left[\sqrt{\frac{1}{p_i^2} + \frac{1}{p_k^2}}\,X\right] \cos\frac{Y}{p_i} \sin\frac{Z}{p_k} \tag{33}$$

Terms with $\sin Y/p_i$ and $\cos Z/p_k$ have been left out in (33), so that the shielding potential is even with respect to $Y$ and odd with respect to $Z$. This corresponds to the case

of a symmetric unwarped current sheet when the dipole tilt $\Psi = 0$.

How can tilt effects, first of all, the warping of the current sheet be taken into account ? Since for $\Psi \neq 0$ the warped current sheet and its field are no longer symmetric with respect to the GSM equatorial plane, we have to include terms with $\cos Z/p_k$ in the potential. In this way, one can obtain an optimal set of parameters for a given value of the dipole tilt $\Psi$. However, this is not a full solution to the problem: we need a shielding field that could be used for arbitrary values of the tilt angle and would have an analytical dependence on $\Psi$. Such a model can be devised by adopting an extended expansion for the scalar potential, in which the coefficients are functions of $\Psi$, for example,

$$U = \sum_{i,k=1}^{N} (a_{ik} + b_{ik}\cos\Psi)\times \exp\left[\sqrt{\frac{1}{p_i^2}+\frac{1}{p_k^2}}\,X\right]\cos\frac{Y}{p_i}\sin\frac{Z}{p_k} + \sum_{i,k=1}^{N} (c_{ik}\sin\Psi + d_{ik}\sin 3\Psi)\times \exp\left[\sqrt{\frac{1}{q_i^2}+\frac{1}{q_k^2}}\,X\right]\cos\frac{Y}{q_i}\cos\frac{Z}{q_k} \qquad (34)$$

The potential (34) is composed of two terms with different symmetries. The first term produces a field with the same symmetry as that of an untilted dipole ($\Psi = 0$), i.e., $B_x$ and $B_z$ are odd and even functions of $Z$, respectively. The second term has the opposite symmetry, corresponding to the field of a dipole with $\Psi = 90°$, so that the $B_x$ component is even and $B_z$ is odd with respect to $Z$. The net shielding field given by the potential (34) satisfies general symmetry conditions [e.g., *Mead and Fairfield*, 1975]

$$\begin{aligned} B_x(X,Y,-Z,\Psi) &= -B_x(X,Y,Z,-\Psi) \\ B_y(X,Y,-Z,\Psi) &= -B_y(X,Y,Z,-\Psi) \\ B_z(X,Y,-Z,\Psi) &= B_z(X,Y,Z,-\Psi) \end{aligned} \qquad (35)$$

Of course, the assumed form of the dependence of $U$ on $\Psi$ in (34) is by no means unique: other appropriate functions could be adopted (e.g., polynomials in $\Psi$), with the requirement that the corresponding factors in the first and second sums be an even and an odd function of $\Psi$, respectively.

With $1 \leq i,k \leq N = 4$, the representation (34) contains 64 unknown coefficients $a_{ik}$, $b_{ik}$, $c_{ik}$, $d_{ik}$, and 8 nonlinear parameters $p_i$ and $q_i$, all of which are found by minimizing the net $\langle \delta B_n^2 \rangle$ over the model boundary.

Three important things should be pointed out here. First, since the shielding potential (34) contains a parametric dependence on the geodipole tilt angle, it is necessary that many different values of $\Psi$ be represented in the sum (6), scattered within a sufficiently wide range. Similarly, to ensure good accuracy of the shielding from the nose region to the far tail, sufficient spatial coverage is needed. In this study, the shielding problem was solved separately for each of the three tail modes by minimizing (6) on a set of 644 points distributed over the model magnetopause between the subsolar point and $X \approx -230\,R_E$. To avoid degeneracy in the inverse problem, which might result in an ill-conditioned system of equations and numerical instabilities, a moderate amount of randomization was introduced both in the location of individual points on the magnetopause and in the corresponding values of the tilt angle $\Psi$.

Second, as noted in section 2.4.1, the field of the cross-tail current was assumed to be the superposition (30) of three modes. For this reason, the "partial" tail-shielding fields $\mathbf{B}_{TS,1}$, $\mathbf{B}_{TS,2}$, and $\mathbf{B}_{TS,3}$ were found separately for the three basic cross-tail modes, $\mathbf{B}_{CT,1}$, $\mathbf{B}_{CT,2}$, and $\mathbf{B}_{CT,3}$, respectively, so that the net shielded tail field

$$\mathbf{B}_T = a_{T,1}(\mathbf{B}_{CT,1} + \mathbf{B}_{TS,1}) + a_{T,2}(\mathbf{B}_{CT,2} + \mathbf{B}_{TS,2}) + a_{T,3}(\mathbf{B}_{CT,3} + \mathbf{B}_{TS,3}) \qquad (36)$$

was kept confined within the magnetopause for any set of individual mode amplitudes $a_{T,1}$, $a_{T,2}$, $a_{T,3}$. This permits one to vary intensities and profiles of the tail current, so that it could be fitted to data without violating the shielding condition.

Third, it would greatly increase the model's flexibility if some nonlinear characteristics of the tail current (for example, the "hinging distance" $R_H$) could be included among the adjustable parameters. However, that would require a reevaluation of the values of $a_{ik}$, $b_{ik}$, $c_{ik}$, $d_{ik}$, $p_i$, and $q_i$, at each iteration, which was not feasible with our computing capabilities. For that reason it was decided to use the initial values of $a_{ik}$, $b_{ik}$, ..., $q_i$ for the whole sequence of the data-fitting iterations and then recalculate them, using the final values of the nonlinear parameters, in order to restore the shielding. In all cases such an adjustment produced only a slight ($\leq 1\%$) increase of the rms deviation of the model field from a data set, so that there was no need for further iterations.

Figure 3 illustrates the shielding of the tail field, for the case of the mode $\mathbf{B}_{CT,1}$ with the longest fall-off scale length, $L = 100\,R_E$. Figures 3a and 3b show the magnetic field lines corresponding, respectively, to the unshielded field (30) of the equatorial current disc and after the addition of the shielding field $\mathbf{B}_{TS,1}$.

As a quantitative measure of the shielding quality, the ratio $Q = [\langle(\delta\mathbf{B}_T \cdot \mathbf{n})^2\rangle]^{1/2}/\max(\mathbf{B}_{CT} \cdot \mathbf{n})$ of the rms residual normal component of the net field to the maximal normal field from the unshielded source was evaluated. For the three tail modes with $L = 100$, $L = 40$, and $L = 15$, the values of $Q$ were found to be 0.83%, 0.64%, and 0.65%, respectively.

### 2.5. Ring Current Module

The ring current module, like the tail module (36), must represent fields from two sources:

$$\mathbf{B}_{RC} = a_{RC}(\mathbf{B}_{RCI} + \mathbf{B}_{RCS}) \qquad (37)$$

The parentheses on the right contain the sum of the field $\mathbf{B}_{RCI}$ produced by the current inside the magnetosphere (i.e., the ring current proper) and the corresponding shielding field $\mathbf{B}_{RCS}$. The sum yields the field of a unit-amplitude shielded ring current, and therefore multiplying it by an arbitrary amplitude factor $a_{RC}$ does not violate the shielding condition.

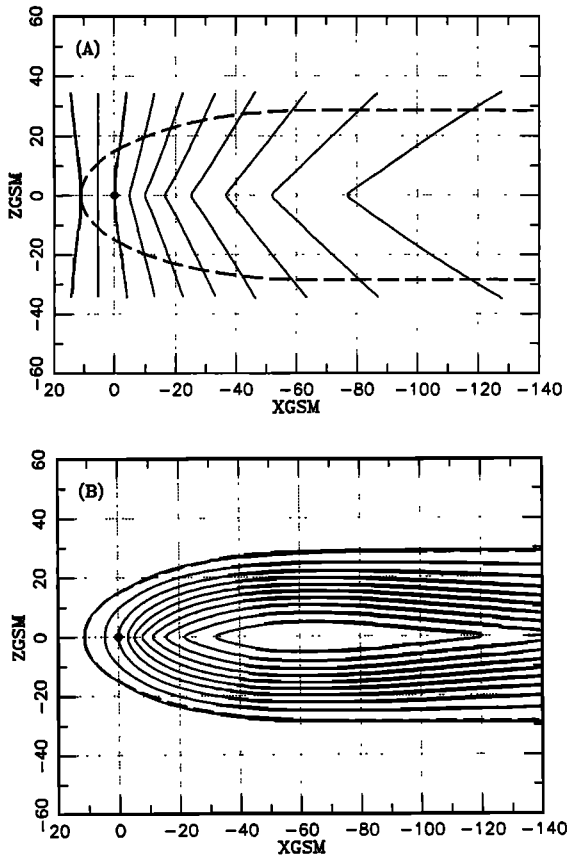


**Figure 3.** Lines of the magnetic field produced by the tail current system: (a) lines of the unshielded field (equation (30)) of the cross-tail current sheet, and (b) net field, including that given by the tail shielding potential (34). In this specific example, the tail field mode with the largest fall-off scale length, $L = 100\,R_E$, is displayed, for zero tilt angle. The model magnetopause is shown by the dashed line in both panels.

The internal ring current term $\mathbf{B}_{\mathrm{RCI}}$ was represented by a vector potential of the form (19), with a special choice of the parameters $f_i$ and $g_i$, so that the radial profile of the current density is confined within a relatively narrow region $R \leq 10$–$12\,R_E$ and has a maximum at 6-8 $R_E$ (see *Tsyganenko and Peredo* [1994] for details). On the basis of our experience with previous models, the ring current thickness was allowed to vary in the day-night direction. We also allowed for a shift of the whole ring current along the X-axis and introduced a scaling of its dimension by some factor, as additional degrees of freedom.

The model ring current was assumed to be centered on the dipole equatorial plane, so that it inclines by the angle $\Psi$ to the GSM equatorial plane, in response to the Earth's dipole tilt.

Let us now consider the shielding term $\mathbf{B}_{\mathrm{RCS}}$. At sufficiently large distances, the field of the ring current becomes close to that of a dipole. Therefore it was decided to try using cylindrical harmonic expansions (section 2.4.2) for approximating the correponding shielding potential. However, because of the distributed nature of the ring current, the zero- and first-order harmonics alone did not provide sufficient accuracy, as they did for the Earth's dipole. For that reason, higher-order terms up to $m$=5 were included, containing in total 60 coefficients and 10 nonlinear scaling parameters. A least squares fitting procedure was again employed, to obtain their optimal values, determining the shielding field $\mathbf{B}_{\mathrm{RCS}}$. For this ring current model, the shielding quality was found to be 1.6%. The shielded ring current field (37) was then included in the model as an independent term, whose parameters were found together with the tail parameters by least squares fitting to spacecraft data.

Figure 4 shows field lines corresponding to the ring current term (37). The slight inward bending of the lines which cross the nightside equatorial plane at large distances is caused by a small residual eastward current, due to incomplete cancellation of separate terms in the expansion (19). This unphysical current, however, does not pose any major problem: in comparison to the large westward current due to the tail terms (36), it is very small.

## 3. Assembling the Model: Data and Least Squares Fitting Criteria

This section describes first results of assembling the above modules into a new global representation of the magnetic field, based on spacecraft data. As in the previous models [*Tsyganenko*, 1987, 1989a], one important component is still missing, the fields of Birkeland current systems. Several attempts have been made recently to develop feasible approximations for the field-aligned current contribution [*Usmanov and Tsyganenko*, 1984; *Tsyganenko*, 1988, 1991, 1993; *Stern*, 1993]. However, we still lack a complete and flexible model for the field from both region 1 and 2 currents; the reader is referred to the papers cited above and/or recent reviews by *Tsyganenko* [1990] and *Stern* [1994] for more detailed discussion.

This paper is focused primarily on the methods for representing the field from various separate internal magnetospheric sources and the corresponding components of the magnetopause current, which ensure their confinement within the boundary. The question of parametrizing the

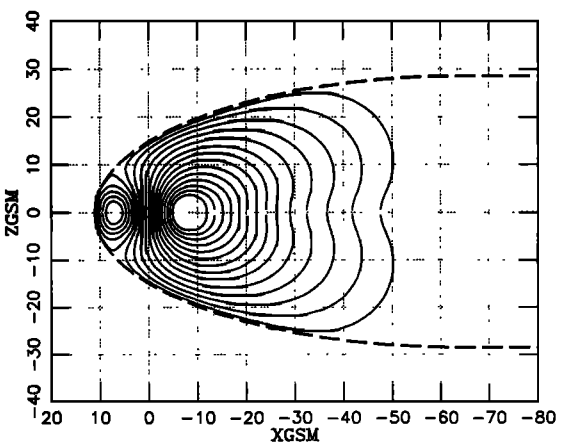


**Figure 4.** Lines of the magnetic field, produced by the shielded ring current, in the case of $\Psi = 0$. A slight inward bending of the outermost field lines in the tail region is a model artifact, resulting from an incomplete cancellation of terms in expansion (19). The model magnetopause is shown by the dashed line.

model by the solar wind pressure and the IMF will be further discussed in section 4; however, a comprehensive treatment of that subject is relegated to a separate work.

In the present study, the new approach was tested by fitting the model parameters to a subset of magnetometer data, corresponding to the relatively narrow range $1.9 < p_{sw} < 2.1$nPa of solar wind pressures. These values of $p_{sw}$ are close to the long-term average for the decade 1964–74 and lie approximately in the middle of the larger interval $1.47 < p_{sw} < 2.60$nPa, corresponding to the chosen values of the model magnetopause parameters. The data set included the IMP and HEOS data used for constructing the earlier 1987 and 1989 models as well as data taken by the ISEE 1 and 2 spacecraft during 1977–1981 [*Fairfield et al.*, 1994]

The magnetic field data set comprised 2949 averages, nonuniformly distributed in the Earth's magnetosphere within the Moon's orbit, as shown in Figure 5. There are very few data tailward of $X = -35\,R_E$, and the density of the points is much higher sunward of $X = -25\,R_E$; more than half of the data in this region came from ISEE measurements.

The net contribution from external sources was taken as the sum of three terms

$$\mathbf{B} = \mathbf{B}_{DS} + \mathbf{B}_T + \mathbf{B}_{RC} \tag{38}$$

The term $\mathbf{B}_{DS}$ is the dipole-shielding field represented by the harmonic expansions (10)–(16) with the parameter values given in Table 1. The terms $\mathbf{B}_T$ and $\mathbf{B}_{RC}$ are the contributions from the self-shielded tail and ring current sources, given by (36) and (37), respectively. Note that the dipole shielding term $\mathbf{B}_{DS}$ does not contain any free parameters which could be derived from data: as soon as the shape and size of the magnetopause are specified, this term becomes fully determined as a unique solution of the boundary problem (4).

Several trial runs were performed, fitting the model (38) to the data with different selections of free parameters. In the end, the following set of 10 variable parameters was adopted for further experiments: (1) the ring current amplitude $a_{RC}$, (2–4) the three amplitudes of tail modes $a_{T,1}$ to $a_{T,3}$, (5) the shift $X_c$ of the tail current system along the $X_{GSM}$ axis, (6–7) the "hinging distance" $R_H$ and the warping amplitude $G$, defining the tilt-dependent transverse shape of the cross-tail current sheet, and (8–10) the parameters $D_0$, $D_1$, and $D_2$, which control the cross-tail current thickness, as defined by (27)–(29). The search for their optimal values was performed in a sequence of iterations, combining a standard linear least squares method for the four amplitudes with the downhill simplex algorithm for the nonlinear parameters. After a few hundred iterations, the parameters given above converged to an optimal set of values, and then a final adjustment of the tail and ring current shielding fields was performed.

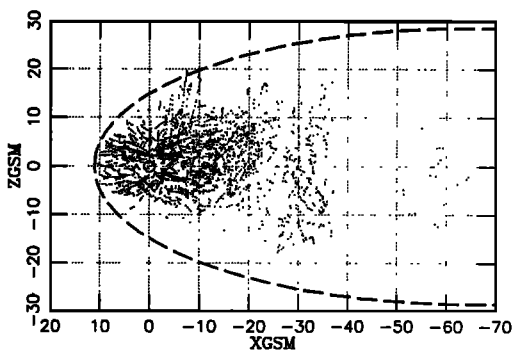


**Figure 5.** Spatial distribution of the data points in the spacecraft data set used for least squares fitting of the model parameters. The data correspond to a narrow interval of the solar wind pressure with $1.9 \le p_{sw} \le 2.1$ nPa and comprise a total of 2949 magnetic field averages, obtained from IMP, HEOS, and ISEE measurements made during 1966–1981.

Tracing field lines in models with the parameters obtained in these early runs showed a discouraging persistent feature: as in the 1989 model, a region with unrealistic small values of equatorial $B_z$ emerged again in the tail current sheet at $10 \le R \le 35\,R_E$. Attempts to remedy the problem by including tail modes with different values of $e$-folding distances or by starting the fitting procedure from different initial values of the parameters did not lead to a satisfactory result. Eventually, it was realized that the source of the problem lies in the least squares fitting criterion. Namely, all the empirical models so far devised fit parameters by unweighted least squares, minimizing

$$\sigma_1 = \sqrt{\sum_{i=1}^{N} [\mathbf{B}_{obs}^{(i)} - \mathbf{B}_{model}^{(i)}]^2 \Big/ N} \tag{39}$$

This criterion provides the "best fit" approximation to the observed distribution of **B** vectors. Obviously, the tail lobe regions with strong **B** are likely to dominate in defining optimal values of the parameters entering in $\mathbf{B}_{model}$. Also, as can be seen in Figure 5, the tail lobes contribute many more data points, since they occupy a larger volume and are better covered by spacecraft orbits. Therefore criterion (39) discriminates against regions of weak magnetic field, in particular, against the "neutral sheet" in the equatorial plasma sheet. However, regions with weak magnetic fields are of crucial importance to the physics, especially for understanding substorm mechanisms. Even small variations of **B** in these regions can lead to significant changes in the predicted field line geometry and hence to large errors in mapping.

The magnetic field vector can be represented as the product of a scalar magnitude and a unit direction vector, $\mathbf{B} = B\,\mathbf{b}$, and only **b** is actually relevant for the mapping procedure! This implies that the mapping accuracy can be increased if, instead of fitting the full vector, **B**, we use the direction vector $\mathbf{b} = \mathbf{B}/B$, so that the quantity to be minimized becomes

$$\sigma_2 = \sqrt{\sum_{i=1}^{N} \left[\mathbf{b}_{obs}^{(i)} - \mathbf{b}_{model}^{(i)}\right]^2 \Big/ N} \tag{40}$$

essentially weighting observations by $1/B$.

This conjecture was confirmed by optimization runs using $\sigma_2$ instead of $\sigma_1$ as the merit function. In all runs employing the new mapping-oriented criterion, it yielded much more robust configurations of the plasma sheet field, with just minor changes in other regions of the magnetosphere. Of course, with perfect data and a model that could accom-

modate any configuration, the model minimizing (39) would also minimize (40), i.e., both criteria would provide the same parameter values. However, real models are not perfect and real data are noisy and nonuniform, which leads to biased parameter values.

Another subtle point is that since criterion (40) emphasizes the field direction and does not explicitly contain its magnitude, one might expect large errors in the latter. Note, however, that the direction vectors $\mathbf{b}^{(i)}$ in (40) are calculated by using the total field, including the Earth's dipole contribution, which is known and hence does not contain variable model parameters. This ensures that the model values of $B$ remain close to the observed ones: a comparison of the models based on the criteria (39) and (40) revealed only a minor (within 10%) difference in the gradient of the near-Earth tail lobe field.

Figure 6 shows two field line configurations, obtained by minimizing (39) and (40) for the same data set with $1.9 < p_{sw} < 2.1$ nPa. Clearly, much more magnetic flux crosses the near-Earth plasma sheet in the second case (plot B), than in the first (plot A). At geocentric distances smaller than $10R_E$, the degree of field line stretching in Figure 6b is close to that given by the 1989 model for $K_p = 2-, 2, 2+$ [*Tsyganenko*, 1989a, Figure 9]. The average $K_p$ value for the data set $1.9 < p_{sw} < 2.1$ nPa is about 2+, which means that the new model provides realistic $B_z$ values both at close and large distances.

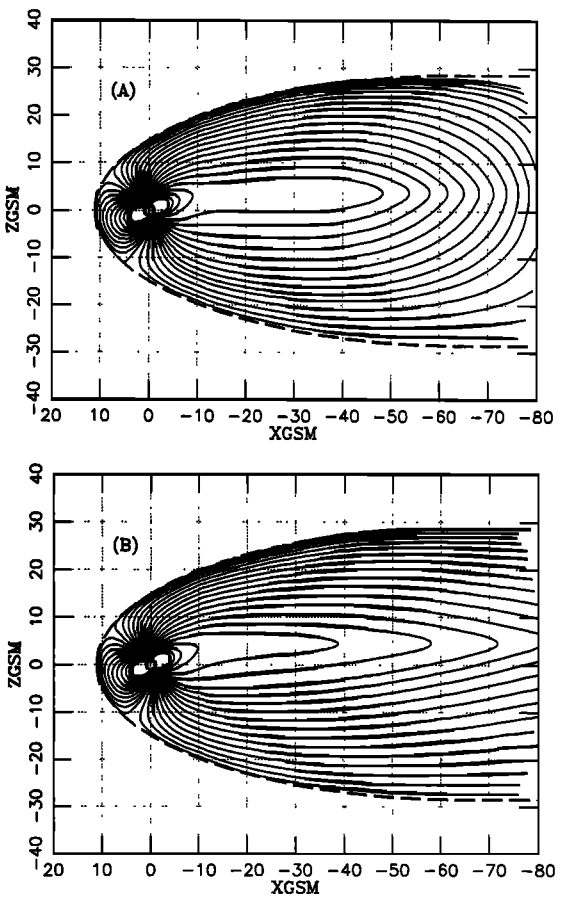


**Figure 6.** Shielded magnetic field line configurations, obtained by calibrating the new model against the data set shown in Figure 5. The dipole tilt angle equals 20°. The two panels display the results of using two different criteria for fitting the model to data: (a) the standard criterion, in which the minimal rms deviation (39) of the model **B** vectors from the measured ones was sought, and (b) the new criterion, in which the rms difference (40) between the model and observed field directions was minimized. Note the significant difference in the amount of the magnetic flux crossing the plasma sheet.

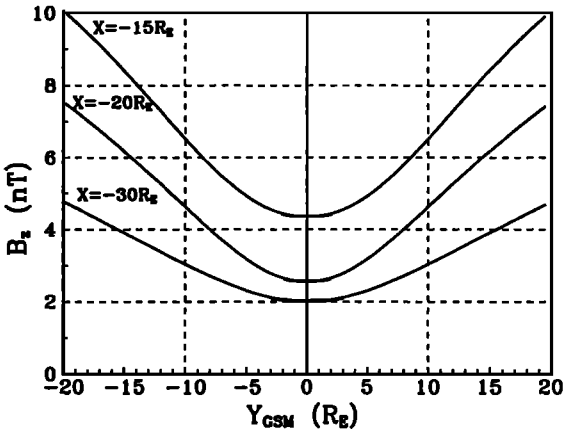


**Figure 7.** Dawn-dusk profiles of the net equatorial $B_z$ in the model, for three different values of $X$. In agreement with *Fairfield* [1986], $B_z$ grows toward the tail's flanks. The plots correspond to the model field illustrated in Figure 6b.

In Figure 7 dawn-dusk profiles of equatorial $B_z$ are shown for three values of $X$. The model values of $B_z$ are much closer to those observed, discussed by *Stern and Tsyganenko* [1992], *Rostoker and Skone* [1993], *Peredo et al.* [1993], *Huang and Frank* [1994]. Also, in accordance with well-established observations [*Fairfield*, 1986], the model $B_z$ increases from the midnight meridian to the tail flanks.

An alternative merit function, which could be used instead of (40) as a measure of mapping quality, is the rms angle between the observed magnetic field and the one given by the model:

$$\sigma_3 = \sqrt{\sum_{i=1}^{N} \left[\cos^{-1}\{\mathbf{b}_{obs}^{(i)} \cdot \mathbf{b}_{model}^{(i)}\}\right]^2 / N} \qquad (41)$$

The merit function (41) gains relatively more contribution from points with a large difference between the model and observed **b** vectors. However, near the optimal values of the model parameters, the overall difference becomes negligible, so that the criteria based on (40) and (41) yield almost the same results.

Finally, it should also be realized that the mapping-oriented criteria based on (40) or (41) are technically more difficult to implement since, in contrast to (39), the amplitudes of the separate current systems enter in (40) and (41) as non-linear parameters, thus increasing the dimensionality of the search algorithm and imposing more restrictions upon the flexibility of the model.

## 4. Discussion

The purpose of this paper is to outline basic principles of the new approach and to illustrate it for a small data set cor-

responding to average solar wind conditions. An important piece of work still remains to be done: calibrating the model by current values of the solar wind pressure and IMF. In this section we will briefly discuss this issue.

Let us consider first the effects of the solar wind dynamic pressure upon the dipolar part of the magnetopause field. The geodipole field and its shielding field $\mathbf{B}_{DS}$ dominate the near-Earth magnetosphere ($|X| < 15\,R_E$) and become negligibly small at larger distances. In this front region, changes in the solar wind pressure $p_{sw} = \rho v^2$ produce self-similar contractions or expansions of the magnetopause [*Sibeck et al.*, 1991; *Roelof and Sibeck*, 1993]. This allows for easy parametrization of $\mathbf{B}_{DS}$ by $p_{sw}$, using a uniform scaling transformation (17) with $\kappa = [p_{sw}/p_{sw}^{(0)}]^{1/6}$.

However, the situation is more complicated with regard to the tail and ring currents. First, the terms $\mathbf{B}_T$ and $\mathbf{B}_{RC}$ contain many free parameters, including four amplitude coefficients and several geometrical factors discussed in section 2.4.1, and these parameters themselves might be affected by $p_{sw}$. It is well known that there is a good correlation between $p_{sw}$ and the magnitude of the tail lobe field [e.g., *Nakai et al.*, 1991]. Therefore we might explore an empirical dependence of the amplitudes $a_{T,1} - a_{T,3}$ of the tail terms (36) on $p_{sw}$, and then fit the model to magnetic field data tagged by simultaneous values of the pressure, considering $p_{sw}$ as an additional input variable, like spatial coordinates or the Earth's dipole tilt angle.

Nonetheless, there still remain at least two reservations. First, the magnetosphere's response to variations of the solar wind pressure is by no means instantaneous and does not occur simultaneously over its whole length. Rather it is likely to be a wave-like reconfiguration, propagating tailward from the dayside. Since the solar wind takes about 10 minutes to pass the near-Earth magnetosphere, while in most cases only hourly averages of $p_{sw}$ are available with the magnetic field data, this implies an inevitable blurring of the correlation between the magnetospheric field and $p_{sw}$. Second, even with averaging over sufficiently long time periods, the global effect of the $p_{sw}$ variations cannot be reduced to self-similar scaling of the magnetopause dimensions. Though there exist quantitative models based on many direct observations of the front part of the boundary [*Sibeck et al.*, 1991; *Petrinec et al.*, 1991; *Roelof and Sibeck*, 1993], much less is known about the tailward magnetopause and its response to varying interplanetary conditions.

There is also strong evidence for IMF influence upon the magnetopause shape and upon its sensitivity to changes of the pressure $p_{sw}$. Again, for the front region of the boundary, the results of *Sibeck et al.* [1991], *Petrinec et al.* [1991], and *Roelof and Sibeck*, [1993] provide a good base for calibrating the models. However, tailward of $X \approx -15\,R_E$, much fewer boundary crossings are available that have simultaneous solar wind observations; indirect methods may be very beneficial in this region. *Petrinec and Russell* [1993] derived the tail magnetopause shapes for different $p_{sw}$ and IMF $B_z$, based on measurements of $B$ inside the tail lobes and an approximate form of the pressure balance equation. Using their results (equations (4)–(5) and Figure 4), it is possible to evaluate the tail radius $R_T$ as a function of $p_{sw}$. For $X_{GSM} = -20\,R_E$ this yields curves which can be nicely fitted by a power law as $R_T = 27.01\,p_{sw}^{-0.224}$ and $R_T = 30.48\,p_{sw}^{-0.248}$ for northward and southward IMF, respectively, in good agreement with an earlier result of *Nakai et al.* [1991], who crudely estimated $R_T \propto p_{sw}^{-0.24}$ (such agreement is not surprising, however, since both *Nakai et al.* [1991] and *Petrinec and Russell* [1993] used the same data and employed the same simplified pressure balance equation for inferring the tail boundary flaring angle). It is more interesting to note a remarkable agreement of their results with that of *Lui* [1986], who measured the tail boundary radius at $-20 < X_{GSM} < -15\,R_E$ using direct observations of the magnetopause crossings by IMP 6 in 1971–73. Fitting the dependence of $\log R_T$ against $\log p_{sw}$ by a straight line, he obtained the slope between –0.22 and –0.23, which is very close to the aforementioned results of *Nakai et al.* [1991] and *Petrinec and Russell* [1993]. The tail radius is thus more sensitive to changes in $p_{sw}$ than is the standoff distance.

The considerations stated above will be taken into account in the next phase of this project, aimed at developing an advanced magnetospheric field model, parametrized by solar wind conditions and some indices which reflect the current state of principal magnetic field sources.

In this work, an axially symmetric surface was employed for the average magnetopause shape. Given a large scatter of the observed magnetopause positions and lack of experimental information on its shape at high latitudes, it makes little sense, at this point, to introduce more refined approximations, taking into account possible deviations from the axial symmetry. However, this issue should be addressed in greater detail in future models, which will be able to take into account distortions of the magnetopause shape due to transient features in the solar wind. Such models should necessarily satisfy the pressure balance at the magnetopause and hence will incorporate axial asymmetry, in particular near the polar cusps. The method described above has much flexibility and appears quite suitable for solving that problem, which is one of the most challenging tasks in magnetospheric physics.

## 5. Summary

1. A compact and flexible six-term analytical representation was developed for the magnetopause field, shielding the Earth's dipole field within a realistically shaped boundary, valid for arbitrary values of the dipole tilt angle and up to large geocentric distances. The coefficients of the scalar potential expansions were computed for several rates of the tailward flaring of the magnetopause; combined with the scaling transformation, this allows the size and shape of the boundary to be easily varied.

2. Similar representations were devised for the magnetopause field components due to the tail and the ring current systems. The tail shielding field is approximated by expansions in rectangular harmonics, while that for the ring current employs combinations of cylindrical harmonics with different scale lengths.

3. Assembling the aforementioned modules and determining their parameters from spacecraft data has provided realistic, fully shielded magnetic field configurations. A new mapping-oriented criterion was used in the optimization procedure: instead of **B** vectors, it fitted unit direction vectors

$\mathbf{B}/B$. The "best fit" modeling, in this sense, implies the best accuracy of mapping; in particular, this allows to eliminate the occurrence of unrealistically small equatorial $B_z$ values and produces a more reliable field line tracing.

**Acknowledgments.** The author is grateful to David Stern, Tom Sotirelis, and Mauricio Peredo for stimulating discussions, careful reading, and many helpful comments on the manuscript. Thanks are also due to both referees for pointing out errors in the earlier version of the manuscript as well as for penetrating comments on some aspects of the fitting criteria.

The Editor thanks S.M. Petrinec and another referee for their assistance in evaluating this paper.

## References

Alekseev, I.I., and V.P. Shabansky, A model of magnetic field in the geomagnetosphere, *Planet. Space Sci., 20,* 117, 1972.

Baker, D.N., T.I. Pulkkinen, R.L. McPherron, J.D. Craven, L.A. Frank, R.D. Elphinstone, J.S. Murphree, J.F. Fennell, R.E, Lopez, and T. Nagai, CDAW 9 analysis of magnetospheric events on May 3, 1986: Event C, *J. Geophys. Res., 98,* 3815, 1993.

Beard, D.B., D. Hirschi, and K. Propp, The tailward magnetopause field beyond 10 Re, *J. Geophys. Res., 87,* 2533, 1982.

Behannon, K.W., Geometry of the geomagnetic tail, *J. Geophys. Res., 75,* 743, 1970.

Bieber, J.W., P. Evenson, and Z. Lin, Cosmic ray trajectories in the Tsyganenko magnetosphere, *Antarctic J. U.S., 27* (5), rev. issue, 318, 1992.

Cao, F., and L.C. Lee, Plasma pressure and anisotropy inferred from the Tsyganenko magnetic field model, *Ann. Geophys., 12,* 286, 1994.

Choe, J.Y., and D.B. Beard, The compressed geomagnetic field as a function of dipole tilt, *Planet. Space Sci., 22,* 595, 1974.

Donovan, E.F., G. Rostoker, and C.Y. Huang, Regions of negative $B_z$ in the Tsyganenko 1989 model neutral sheet, *J. Geophys. Res., 97,* 8697, 1992.

Elphinstone, R.D., D. Hearn, J.S. Murphree, and L.L. Cogger, Mapping using the Tsyganenko long magnetospheric model and its relationship to Viking auroral images, *J. Geophys. Res., 96,* 1467, 1991.

Fairfield, D.H., Average and unusual locations of the Earth's magnetopause and bow shock, *J. Geophys. Res., 76,* 6700, 1971.

Fairfield, D.H., The magnetic field of the equatorial magnetotail from 10 to 40 $R_e$, *J. Geophys. Res., 91,* 4238, 1986.

Fairfield, D.H., An evaluation of the Tsyganenko magnetic field model, *J. Geophys. Res., 96,* 1481, 1991.

Fairfield, D.H., N.A. Tsyganenko, A.V. Usmanov, and M.V. Malkov, A large magnetosphere magnetic field database, *J. Geophys. Res., 99,* 11,319, 1994.

Howe, H.C., and J.H. Binsack, Explorer 33 and 35 plasma observations of magnetosheath flow, *J. Geophys. Res., 77,* 3334, 1972.

Huang, C.Y., and L.A. Frank, Magnitude of $B_z$ in the neutral sheet of the magnetotail, *J. Geophys. Res., 99,* 73, 1994.

Lui, A.T.Y., Solar wind influence on the magnetotail configuration and dynamics, *Solar Wind–Magnetosphere Coupling*, edited by Y. Kamide and J.A. Slavin, p.671, Terra Scientific, Tokyo, 1986.

Maezawa, K., Magnetotail boundary motion associated with geomagnetic substorms, *J. Geophys. Res., 80,* 3543, 1975.

Mead, G.D., Deformation of the geomagnetic field by the solar wind, *J. Geophys. Res., 69,* 1181, 1964.

Mead, G.D., and D.B. Beard, Shape of the geomagnetic field–solar wind boundary, *J. Geophys. Res., 69,* 1169, 1964.

Mead, G.D., and D.H. Fairfield, A quantitative magnetospheric model derived from spacecraft magnetometer data, *J. Geophys. Res., 80,* 523, 1975.

Midgeley, J.E., and L. Davis Jr., Calculation by a moment technique of the perturbation of the geomagnetic field by the solar wind, *J. Geophys. Res., 68,* 5111, 1963.

Nakai, H., Y. Kamide, and C.T. Russell, Influences of solar wind parameters and geomagnetic activity on the tail lobe magnetic field: a statistical study, *J. Geophys. Res., 96,* 5511, 1991.

Peredo, M., D.P. Stern, and N.A. Tsyganenko, Are existing magnetospheric models excessively stretched?, *J. Geophys. Res., 98,* 15343, 1993.

Petrinec, S.M., and C.T. Russell, An empirical model of the size and shape of the near-Earth magnetotail, *Geophys. Res. Lett., 20,* 2695, 1993.

Petrinec, S.M., P. Song, and C.T. Russell, Solar cycle variations in the size and shape of the magnetopause, *J. Geophys. Res., 96,* 7893, 1991.

Press, W.H., B.P. Flannery, S.A. Teukolsky, and W.T. Vetterling, *Numerical Recipes*, Cambridge University Press, New York, 1992.

Pulkkinen, T.I., D.N. Baker, D.N. Fairfield, R.J. Pellinen, J.S. Murphree, R.D. Elphinstone, R.L. McPherron, J.F. Fennell, R.E. Lopez, and T. Nagai, Modeling the growth phase of a substorm using the Tsyganenko model and multi-spacecraft observations: CDAW-9, *Geophys. Res. Lett., 18,* 1963, 1991.

Roelof, E.C., and D.G. Sibeck, Magnetopause shape as a bivariate function of the interplanetary magnetic field $B_z$ and solar wind dynamic pressure, *J. Geophys. Res., 98,* 21421, 1993.

Rostoker, G., and S. Skone, Magnetic flux mapping considerations in the auroral oval and the Earth's magnetotail, *J. Geophys. Res., 98,* 1377, 1993.

Schulz, M., and M. McNab, Source-surface model of the magnetosphere, *Geophys. Res. Lett., 14,* 182, 1987.

Sibeck, D.G., R.E. Lopez, and E.C. Roelof, Solar wind control of the magnetopause shape, location, and motion, *J. Geophys. Res., 96,* 5489, 1991.

Sotirelis, T., N.A. Tsyganenko, and D.P. Stern, A method for confining the magnetic field of the cross-tail current inside the magnetosphere, *J. Geophys. Res., 99,* 19393, 1994.

Spence, H.E., M.G. Kivelson, and R.J. Walker, Static magnetic field models consistent with nearly isotropic plasma pressure, *Geophys. Res. Lett., 14,* 872, 1987.

Stern, D.P., Parabolic harmonics in magnetospheric modeling: The main dipole and the ring current *J. Geophys. Res., 90,* 10,851, 1985.

Stern, D.P., A simple model of Birkeland currents, *J. Geophys. Res., 98,* 5691, 1993.

Stern, D.P., The art of mapping the magnetosphere, *J. Geophys. Res., 99,* 17,169, 1994.

Stern, D.P., and N.A. Tsyganenko, Uses and limitations of the Tsyganenko magnetic field models, *Eos Trans. AGU, 73,* 489, 1992.

Toffoletto, F.R., R.V. Hilmer, T.W. Hill, and G.-H. Voigt, Solution of the Chapman-Ferraro problem with an arbitrary magnetopause, *Geophys. Res. Lett., 21,* 621, 1994.

Tsyganenko, N.A., Global quantitative models of the geomagnetic field in the cislunar magnetosphere for different disturbance levels, *Planet. Space Sci., 35,* 1347, 1987.

Tsyganenko, N.A., Quantitative model of the system of field-aligned magnetospheric currents, *Geomagn. Aeron.*, Engl. Transl., *28,* 331, 1988.

Tsyganenko, N.A., A magnetospheric magnetic field model with a warped tail current sheet, *Planet. Space Sci., 37,* 5, 1989a.

Tsyganenko, N.A., A solution of the Chapman-Ferraro problem for an ellipsoidal magnetopause, *Planet. Space Sci., 37,* 1037, 1989b.

Tsyganenko, N.A., Quantitative models of the magnetospheric magnetic field: Methods and results, *Space Sci. Rev., 54,* 75, 1990.

Tsyganenko, N.A., Methods for quantitative modeling of the magnetic field from Birkeland currents, *Planet.Space Sci., 39,* 641, 1991.

Tsyganenko, N.A., A global analytical representation of the magnetic field produced by the region 2 Birkeland currents and the partial ring current, *J. Geophys. Res., 98,* 5677, 1993.

Tsyganenko, N.A., and M. Peredo, Analytical models of the magnetic field of disk-shaped current sheets, *J. Geophys. Res., 99,* 199, 1994.

Tsyganenko, N.A., and A.V. Usmanov, Determination of the magnetospheric current system parameters and development of experimental geomagnetic field models based on data from IMP and HEOS satellites, *Planet. Space Sci., 30,* 985, 1982.

Usmanov, A.V., and N.A. Tsyganenko, Taking account of the magnetic effects of the partial ring current system in quantitative modeling of the magnetospheric field, *Geomagn. Aeron.,* Engl. Transl., *24,* 796, 1984.

Voigt, G.H., A three-dimensional analytical magnetospheric model with defined magnetopause, *Z. Geophys., 38,* 318, 1972.

Voigt, G.H., A mathematical magnetospheric field model with independent physical parameters, *Planet. Space Sci., 29,* 1, 1981.

---

N. A. Tsyganenko, Laboratory for Extraterrestrial Physics, Code 695, NASA Goddard Space Flight Center, Greenbelt, MD 20771. (e-mail: ys2nt@lepvax.gsfc.nasa.gov)

(Received August 19, 1994; revised November 28, 1994; accepted November 30, 1994.)